Optimization of vascular-targeting drugs in a computational model of tumor growth

Jana Gevertz*
Department of Mathematics and Statistics, The College of New Jersey, Ewing, New Jersey 08628, USA
(Received 18 November 2011; published 19 April 2012)

A biophysical tool is introduced that seeks to provide a theoretical basis for helping drug design teams assess the most promising drug targets and design optimal treatment strategies. The tool is grounded in a previously validated computational model of the feedback that occurs between a growing tumor and the evolving vasculature. In this paper, the model is particularly used to explore the therapeutic effectiveness of two drugs that target the tumor vasculature: angiogenesis inhibitors (AIs) and vascular disrupting agents (VDAs). Using sensitivity analyses, the impact of VDA dosing parameters is explored, as is the effects of administering a VDA with an AI. Further, a stochastic optimization scheme is utilized to identify an optimal dosing schedule for treatment with an AI and a chemotherapeutic. The treatment regimen identified can successfully halt simulated tumor growth, even after the cessation of therapy.

DOI: 10.1103/PhysRevE.85.041914 PACS number(s): 87.19.xj, 87.55.de, 87.55.Gh, 87.55.K−

I. INTRODUCTION

The vascular needs of a solid tumor are maintained through a combination of tumor co-option of existing host blood vessels and the process of angiogenesis, the growth of new blood vessels from existing ones. Angiogenesis is a rapidly occurring and efficient way for tumors to receive oxygen and nutrients [1]. However, the rapid nature of the process leaves angiogenic vessels limited time to mature in the way normal vessels mature, resulting in an unstable vascular network that tends to be leaky, highly tortuous, and express a different range of proteins than the normal vasculature [1,2]. Given the differences between the normal and angiogenic vasculature, drug developers have been able to design compounds that selectively target the angiogenic vasculature and have minimal impact on the normal tissue vasculature [1,2].

These vascular-targeting compounds fall into two general categories: the angiogenesis inhibitors (AIs) and the vascular disrupting agents (VDAs). AIs are compounds designed to inhibit the tumor-initiated angiogenic process, thereby limiting the oxygen and nutrient supply of the tumor [2]. Hundreds of AIs, each with a unique mode of action, have been or are undergoing clinical trial testing. One AI called bevacizumab (Avastin) has been approved by the U.S. Food and Drug Administration for use with other drugs to treat a range of cancers. The drug has shown to transiently inhibit tumor growth and increase progression-free survival times, although tumor regrowth inevitably occurs after several months of treatment [3].

VDAs are compounds designed to cause the rapid and selective shutdown of tumor-associated blood vessels [1,2], thereby causing cancer cell death. VDAs are not as highly represented in clinical trials as AIs, although there are a handful of VDAs, including combretastatin A4 phosphate (CA4P), that are currently undergoing clinical trial testing [4]. Preclinical studies with CA4P and other VDAs have shown that within 1 h of drug administration, blood flow through the tumor is reduced to levels less than 5% the starting value, and this triggers tumor cell death in about 95% of the tumor mass [1]. However, a thin rim of cancer cells survive at the tumor periphery, limiting the antitumor activity of this class of drugs [1].

Armed with this clinical and preclinical data, Gevertz tested the ability of a hybrid cellular automaton (HCA) model to predict the antitumor activity of an AI, an AI with cytotoxic chemotherapy, and a VDA [5]. Importantly, all model predictions apply to tumors growing in a well-vascularized environment like the brain. For tumors growing in this setting, the biophysical model proved that it can capture the most important features of vascular-targeting therapies. In particular, the model predicted that AIs trigger only transient tumor growth inhibition [5]. It was also found that coupling an AI with a cytotoxic chemotherapeutic can lead to periods of significant tumor shrinkage, but the limited amount of time both the cytotoxic agent and AI can be administered prevents the therapy from being curative in the long term [5]. Finally, it was shown that the simulated VDA, administered once every 3 weeks as done in clinical trials, had relatively little antitumor activity. The HCA model suggested two reasons for VDA inefficacy: (1) a thin rim of proliferative cells survive at the tumor periphery and (2) during the 3-week period of no VDA administration, angiogenesis rapidly occurs and rescues the suffocating tumor, allowing a period of tumor shrinkage to be followed by a period of rapid tumor growth [5]. Taken together, the HCA model proved to accurately predict the qualitative responses of tumor growth to a range of vascular-targeting therapies.

In this paper, an exploration of how the validated HCA model can be used to make novel predictions about cancer treatment is undertaken. In this regard, the model is being used to complement the time consuming, expensive, and risky drug-development process [6,7]. Using the model's predictions, drug developers can make informed decisions about what compounds are worthy of their resources, time, and money, therefore maximizing the likelihood of success while minimizing patient risk. The use of mathematical and computational physics techniques to complement our understanding of drug function, action, and dosing is not a novel one. Pharmacokinetic (PK) models and pharmacodynamic (PD) models have been utilized for decades to determine the

*gevertz@tcnj.edu

relationship between drug dose and response. PK, PD, and combination PK/PD models are widely used in preclinical trials to support drug discovery, interpret toxicity data, and determine optimal dosing strategies [8–13]. More recently, these models have been used in combination with tumor growth models to simultaneously study drug dynamics and tumor response [14,15]. Models have also been used to further our understanding of therapy efficacy [14,16–20], its dependence on and interactions with the immune system [21,22], the transport of chemotherapeutic agents [23–26], and the development of drug resistance [27–30]. Similarly, computational physics models have been employed to better understand radiotherapy. For instance, biophysical models have explored the effects of oxygen levels [31], optimal radiation dosing and scheduling [32], and the combined effects of radiotherapy and chemotherapy [33].

A number of treatment-related models have particularly focused on one class of vascular-targeting compounds, the AIs. Pioneering work in this area was done by Agur and colleagues. Working with a temporal model of tumor cell proliferation, angiogenesis, and vessel maturation, they modeled the influence of angiogenesis-directed treatments, both in isolation and in combination with antimaturation drugs. Simulations suggested that the combination of an AI and an antimaturation drug has significantly more antitumor activity than a stand-alone AI [34]. Following this work, several other researchers began using temporal models to explore the impact of antiangiogenic therapies, including work by Ergun and colleagues [35], d'Onofrio and Gandolfi [36], and Ledzewicz and Schättler [37]. More recently, spatiotemporal models of cancer progression have been used to model antiangiogenic therapy. Kohandel and colleagues developed a reaction-diffusion model of tumor-vasculature interactions and used this model to study the effects of radiation, antiangiogenic therapies, and their combination. Looking at three dosing schedules, they found the sequence of AI administration followed by radiation to be the most effective [38]. Panovska, Byrne, and Maini developed a nonlinear partial differential equation model of healthy cell, tumor cell, and tumor-vasculature evolution. Numerical simulations suggested that a drug that targets an angiogenic stimulant, or the tumor vasculature itself, cannot eliminate the tumor, although under optimal circumstances, tumor growth can be retarded. If such drugs are coupled with an antiproliferative therapy, the tumor can be eliminated [39]. Work by Hinow and colleages [40] studied tumor treatment with a vascular endothelial growth factor (VEGF) inhibitor, both in isolation and with a drug that targets proliferating cells, also using a partial differential equations model. Unlike the other models, this model including both the proliferation and motility of endothelial cells. They discovered that, while antiangiogenic treatments can reduce the size of a tumor mass and slow down cancer cell invasion, this outcome is more dependent on the antiproliferative effects of the drug on endothelial cells than the antimotility effects [40]. Each of these continuous models revealed new aspects of antiangiogenesis treatment. Unlike the other models, the biophysical model presented herein is a hybrid-discrete model, and focuses on tumor-vasculature evolution in a well-vascularized growth environment. Further, in this work, the effects of both AIs and VDAs are explored.

In particular, the HCA model previously developed by Gevertz and colleagues [5,41,42] is utilized herein to explore the following questions about cancer treatment with vascular-targeting drugs.

(1) Can a dosing strategy for the VDA be identified that has more antitumor activity than the suggested protocol of administering the drug once every 3 weeks?

(2) Are there any advantages of adding a VDA to an AI treatment protocol? Preclinical trials suggest their may be some benefit to administering an AI and VDA in tandem, but clinical trials have not yet yielded conclusive results [2].

(3) Can a novel delivery regimen be identified that achieves maximal active tumor cell death using a combination of an AI and cytotoxic chemotherapeutic?

An analysis of the model's predictions and shortcomings is followed up by a discussion on how the results can influence both cancer treatment and the drug-development process.

II. BIOPHYSICAL MODEL AND METHODS

A. Hybrid cellular automaton model of vascular tumor growth

The HCA model utilized in this paper was developed to simulate the growth of a particular type of brain cancer called glioblastoma multiforme (GBM), although the model can be applied to most tumors growing in a vascular environment. For tumors growing in a vascularized environment such as the brain, the co-option-regression-growth experimental model of tumor-vasculature evolution has been proposed [43]. In this model, as a tumorous mass grows, the cancer cells co-opt the mature blood vessels of the surrounding tissue. While many proteins contribute to the mature phenotype of the normal vasculature, angiopoietin-1 (Ang-1) is one protein that plays an important role in vessel maturity [44]. As a tumor mass grows and co-opts the blood vessels of healthy tissue, the naturally occurring antagonist of Ang-1, angiopoietin-2 (Ang-2), is thought to be upregulated by both the tumor and the surrounding microenvironment [43]. Given that Ang-2 is an antagonist to Ang-1, it competes for binding to the common receptor Tie-2 and is responsible for the destabilization of the vasculature [43]. The fate of an unstable blood vessel depends on the presence of a third protein, VEGF. VEGF functions as a potent permeability-inducing agent, an EC chemotactic agent, an EC proliferative factor, and an antiapoptotic signal for ECs [45].

Figure 1 gives a brief summary of the previously developed HCA model of tumor growth in a vascular environment. The first thing the model does is provide the initial conditions for the system: A discrete grid of automaton cells is generated to represent the biological cells, and a discrete network of blood vessels (in particular, the capillaries) is overlaid on top of the automaton cells in order to provide these cells with oxygen and nutrients. To set the algorithm in motion, a single automaton cell is denoted as a proliferative (actively dividing) cancer cell, and vessel response to the presence of the cancer cell is determined by solving a system of partial differential equations (PDEs) that governs the evolution of Ang-1, Ang-2, VEGF, their receptors, and the ligand-receptor complexes. For the ligands Ang-1, Ang-2, and VEGF, the equations account for a production term, linear decay term,

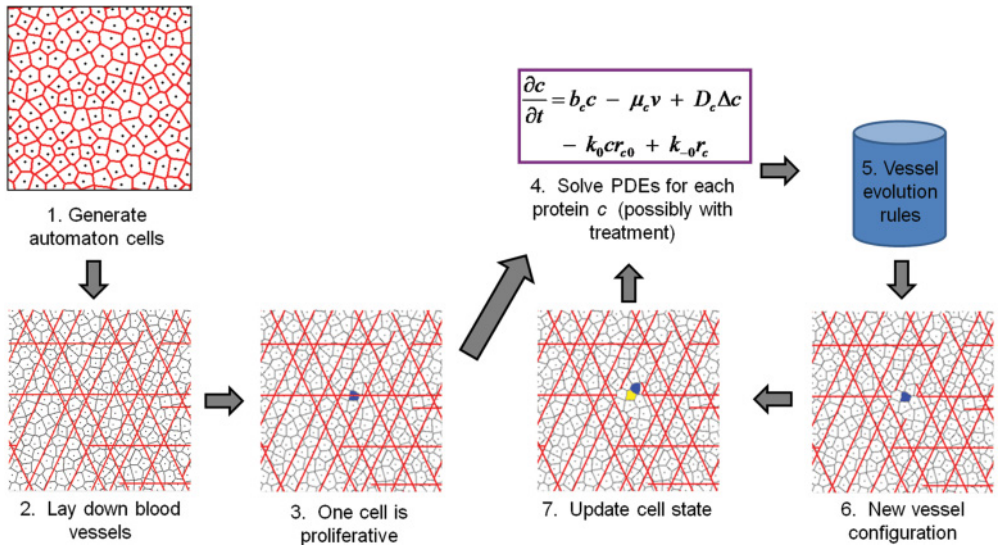

FIG. 1. (Color online) Summary of the HCA model used in this paper to test the efficacy of several vascular-targeting treatment strategies. Viable nonmalignant cells are white, nonproliferative/hypoxic tumor cells are yellow (light gray in black and white), and proliferative tumor cells are blue (dark gray in black and white).

binding of the ligand to its receptor and the breakdown of the ligand-receptor complex. Further, a diffusion term is included for VEGF and Ang-2, although not for Ang-1 since it is thought to act in a paracrine manner [46]. A schematic of the interactions between the growth factors, receptors, ligands, ligand-receptor complexes represented in the PDEs is provided in Fig. 2. The concentration profile of ligands and receptors that results from numerically solving the PDEs one day forward in time is input into a set of biologically inspired rules, and the output is the change in blood vessel configuration. The

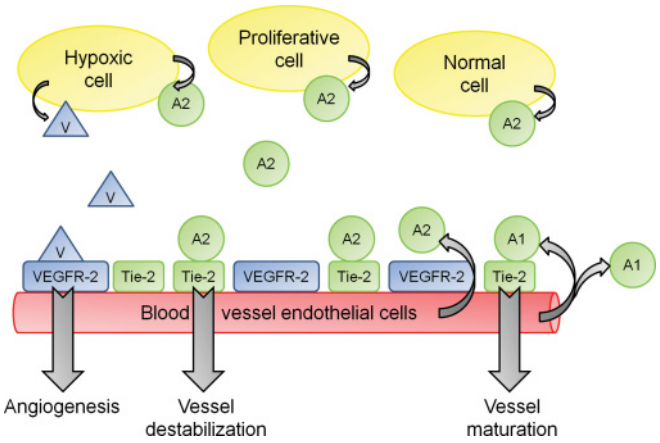

FIG. 2. (Color online) Schematic representation of the system of PDEs detailed in Eqs. (A1)–(A8), showing the interactions between growth factors, receptors, ligand-receptor complexes, and cell types. The ligand VEGF is denoted by V, Ang-1 by $A1$, and Ang-2 by $A2$. Curved arrows indicate the cell type that produced the referenced protein (for instance, hypoxic cells produce VEGF and Ang-2, whereas ECs produce Ang-1 and Ang-2), and straight arrows indicate the physiological response to ligand-receptor binding (for instance, VEGF binding to VEGFR-2 induces angiogenesis). Notice how VEGF and Ang-2 diffuse in the extracellular space, whereas Ang-1 only acts locally.

configuration of blood vessels determines the oxygen level of each cell and therefore determines whether each cancerous automaton cell is proliferative, hypoxic (low-oxygen state), or necrotic (dead). As the tumor grows, treatment may or may not be applied on a given day, depending on the protocol being tested [5]. All simulations were run on a single server consisting of 2 × 2.8-GHz quad-core processors with 24GB RAM.

The focus of this work is performing local sensitivity analyses to dosing levels and schedule and applying optimization strategies grounded in computational physics to exploit the predictive abilities of the HCA model. Therefore, in the following sections, the details related to these analyses are explained. Details on the algorithm itself, which have been published elsewhere [5], have been relegated to the Appendix.

B. Treatment protocols

Three different therapies will be utilized in this paper: an AI, a VDA, and a cytotoxic chemotherapeutic. These drugs are administered in the following fashion.

(1) *AI administration*. A bevacizumab-like AI is simulated by inhibiting the production of VEGF by a factor of T_1, $10 \leqslant T_1 \leqslant 1000$. Clinical and experimental data suggest that one dose of AI allows therapeutic levels to be sustained in the tissue for a 2-to-3-week period of time [47]. Therefore, consistent with clinical protocol, the simulated AI will be administered once every 2 weeks, with therapeutic levels of the drug remaining in the tumor for a 2-week period of time following drug administration.

(2) *VDA administration*. A CA4P-like VDA is simulated by assuming that during each period of drug administration, a VDA destroys an angiogenic blood vessel with probability T_3, $0.3 \leqslant T_3 \leqslant 0.9$. In Phase I clinical trials, CA4P was administered intravenously once every 3 weeks [4], and preclinical trials have shown that maximal vascular shutdown occurs 4–6 h after exposure, with sustained activity for up to

24 h [4]. Thus, to initially model VDA administration, the simulated drug will be given once every 3 weeks, and the drug will only exert its effects on the vasculature the day that it is administered.

(3) *Cytotoxic chemotherapeutic administration.* A temozolomide-like cytotoxic chemotherapeutic is simulated by allowing the agent to kill a certain proportion (T_2) of proliferative cancer cells each day the drug is administered. It has been shown that a continuous administration schedule for temozolomide can be sustained for 6 to 7 weeks [48]. Therefore, in the model the cytotoxic chemotherapeutic can be administered for, at maximum, a consecutive 6-week period of time. Further, using the fractional kill hypothesis and experimental data, it has been estimated previously that $T_2 \approx 0.34$ [5].

The first set of simulations that will be discussed explores the impact of VDA dosing schedule and the efficacy of a VDA/AI drug cocktail. This will involve a local sensitivity analysis on both treatment parameters T_1 and T_3, as well as a sensitivity analysis of the dosing schedule for the VDA. In the second set of simulations, a stochastic algorithm will search for the optimal dosing schedule of an AI and a cytotoxic chemotherapeutic. For all sets of parameters tested, ten simulations will be run and the average tumor response to the drug will be reported. Each treatment is applied once the tumor attains a radius of 4 mm.

C. Stochastic optimization of AI plus cytotoxic drug treatment protocol

In order to identify a treatment protocol that maximizes active tumor cell death, a simulated annealing method is utilized. Simulated annealing is a stochastic optimization method grounded in computational physics that starts with an initial set of parameters and proceeds to evolve the parameters until a desired system property is attained. The parameters are typically evolved using random perturbations, and a scheme is implemented to determine whether each newly generated parameter set should be accepted (as important progress in identifying the optimal solution) or rejected [49]. Putting this in the context of identifying an optimal treatment protocol, the simulated annealing algorithm begins with an initial treatment parameter set. This parameter set specifies the number of days that each drug of interest is given in isolation or in combination with another drug. Starting with this parameter set, the algorithm proceeds to find a new treatment regimen (defined by its parameter set) that only leaves behind a specified small number of active (proliferative plus hypoxic) cancer cells.

To provide more detail, the goal is to minimize the number of active tumor cells remaining after cancer treatment. A function $\Lambda(t)$ is defined to be the average number of active tumor automaton cells left after t days of treatment. In the model, one automaton cell represents approximately seven biological cells [41]. Ideally, the target number of active tumor cells left after applying treatment is zero. So, the goal is to evolve the system from an initial treatment regimen to an optimal one where zero cancer cells remain after treatment. In other words, the goal is to minimize the fictitious "energy" E defined as

$$E = [\Lambda(t) - 0]^2 . \tag{1}$$

Note that given the way the energy function is defined, minimizing E is equivalent to minimizing $\Lambda(t)$:

$$\min[E] \equiv \min[\Lambda(t)]. \tag{2}$$

To initialize the simulated annealing scheme, a set of initial parameters, specifying the number of days different drugs are maintained at therapeutic levels, must be chosen. The following 8-week treatment protocol is used as the starting point for the simulated annealing method.

(1) Days 1–28 of treatment: Maintain therapeutic levels of AI only ($\lambda_{AI} = 28$ is the number of days in the 8-week treatment protocol that therapeutic levels of AI are maintained in the tissue without administering any other form of therapy).

(2) Days 29–56 of treatment: Therapeutic levels of AI plus cytotoxic chemotherapy ($\lambda_{AIC} = 28$ is the number of days in the 8-week treatment protocol that the AI and chemotherapeutic are simultaneously maintained at therapeutic levels in the tissue).

A third treatment parameter is also utilized in the algorithm. This parameter, λ_C, represents the number of days in the 8-week treatment protocol that only the chemotherapy is maintained at therapeutic levels in the tissue; initially, $\lambda_C = 0$. This baseline 8-week treatment regimen (with $\lambda_{AI} = 28$, $\lambda_{AIC} = 28$, and $\lambda_C = 0$) is twice administered to ten growing tumors, for a total of 112 days of treatment for each of the ten tumors. From these simulations, the average number of surviving cancer cells post-treatment is calculated.

The goal of the simulated annealing scheme is to evolve the three parameters (λ_{AI}, λ_{AIC}, and λ_C) until E is minimized. In this context, we are trying to find a drug dosing schedule that leaves zero active cancer cells remaining after $t = 112$ days of treatment. This parameter evolution occurs by randomly perturbing λ_{AI} by t_1 and λ_{AIC} by t_2:

$$\lambda_{AI} \to \lambda_{AI} + t_1, \tag{3}$$

$$\lambda_{AIC} \to \lambda_{AIC} + t_2, \tag{4}$$

where $t_1, t_2 \in \{t \in \mathbb{Z} : -4 \leqslant t \leqslant 4\}$. In order to ensure that the treatment cycle remains 8 weeks long, the value of λ_C is also updated:

$$\lambda_C \to \lambda_C - t_1 - t_2. \tag{5}$$

Further, the choice of perturbation parameters t_1 and t_2 can only be considered if

$$\lambda_{AI}, \lambda_{AIC}, \lambda_C \geqslant 0, \tag{6}$$

$$\lambda_{AIC} + \lambda_C \leqslant 36. \tag{7}$$

The first constraint on the perturbation is required because a drug cannot be administered for a negative number of days. The second constraint comes from the fact that the cytotoxic chemotherapeutic being simulated is temozolomide, and this drug can only be safely tolerated for 6 to 7 weeks at a time [48]. Thirty-six days was intentionally chosen to be below this maximum threshold, as the 8-week treatment protocol will be administered to the patient more than one time.

Once a new treatment parameter set is generated through the perturbation process, it is applied to ten growing tumors for $t = 112$ days (two iterations of the 8-week cycle) and the average number of active tumor cells remaining after 112 days is recorded as $\widehat{\Lambda}(t)$. The difference between the number of surviving active cancer cells from the previous parameter set to the new parameter set is then calculated:

$$\Delta\Lambda = \widehat{\Lambda}(t) - \Lambda(t). \tag{8}$$

Whether the new parameter set gets accepted or rejected depends on $\Delta\Lambda$. The probability of acceptance is defined using the Metropolis acceptance rule [49]:

$$p(\Delta\Lambda) = \begin{cases} 1, & \Delta\Lambda \leqslant 0, \\ \exp(-\Delta\Lambda/T), & \Delta\Lambda > 0, \end{cases} \tag{9}$$

where T is a fictitious "temperature" [49]. Equation (9) says that whenever a new parameter set yields less surviving active cancer cells than the prior parameter set ($\Delta\Lambda < 0$), the change in the parameter values is accepted. When the new parameter set increases the number of surviving cancer cells ($\Delta\Lambda > 0$), the probability of accepting this parameter set is nonzero. The reason the algorithm occasionally accepts moves that increase the number of surviving active tumor cells is to prevent convergence to a local minimum. However, to ensure the algorithm does not continually accept these uphill moves, the temperature T is set to be a monotonically decreasing function of the annealing step k that satisfies

$$\lim_{k\to\infty} T(k) = 0. \tag{10}$$

Therefore, as the number of parameter sets (which is equal to k) tested increases, the likelihood of accepting an uphill move decreases. The cooling schedule used for $T(k)$ is

$$T(k) = 51.5(0.94)^k. \tag{11}$$

The treatment parameter set is perturbed using the specified approach at each annealing step, and the parameter set is accepted with probability $p(\Delta\Lambda)$. This process is continued until the energy of the system [that is, $\Lambda(t)$] approaches its desired value $\Lambda(t) = 0$, within a specified tolerance. In the simulations that follow, the simulated annealing scheme is said to have converged when

$$\Lambda(112) \leqslant 2. \tag{12}$$

In other words, the algorithm has converged when, on average, there are less than two active cancer automaton cells (approximately 15 active cancer cells) remaining in the simulated tumors after two applications of an 8-week treatment protocol.

III. RESULTS AND DISCUSSION

A. VDA dosing and drug cocktails

Preclinical and clinical data have suggested that administering a VDA once every 3 weeks is a relatively ineffective cancer treatment, at least in comparison to AIs. In Gevertz [5], the HCA model used herein validated that, in spite of several simplifications about the vasculature and the mode of drug delivery, it could predict the relative inefficacy of VDAs compared to AIs. According to the model, the limited antitumor activity of VDAs is a result of (1) cancer cells surviving at the tumor periphery and (2) angiogenesis erasing some of the tumor shrinkage that results from VDA-initiated vessel collapse. Therefore, it is natural to ask whether this is a shortcoming of VDAs in general, or if this is a result of the preclinically recommended dosing procedure in which a VDA is administered once every 3 weeks. This is a question that is much quicker, cheaper, and easier to explore in a biophysical model than in clinical trials.

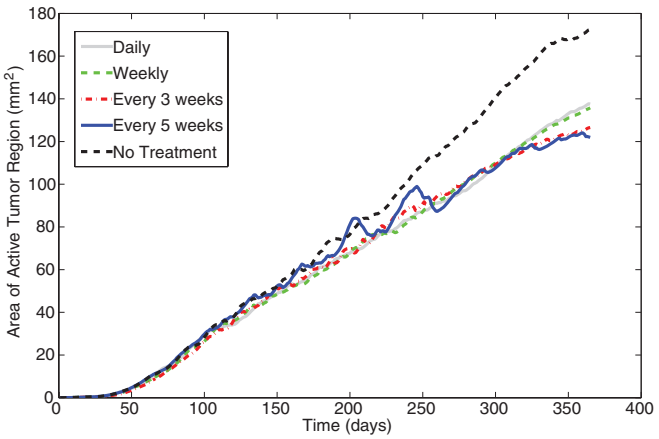

FIG. 3. (Color online) Average active tumor area for four VDA dosing strategies (with $T_3 = 0.6$): daily administration, weekly administration, administration once every 3 weeks, administration once every 5 weeks. Tumor growth is compared to the case where no treatment is administered.

Therefore, assuming that the simulated VDA has a 60% chance of destroying an angiogenic vessel ($T_3 = 0.6$), a comparison of the antitumor activity of a VDA administered daily, weekly, once every 3 weeks, and once every 5 weeks is undertaken (Fig. 3). Quite counterintuitively, the model predicts that the VDA administration schedule has little to no bearing on treatment efficacy. All VDA protocols tested compare favorably to using no treatment whatsoever, but whether the VDA is administered daily or once every 5 weeks does not seem to significantly influence its antitumor activity (Fig. 3). On an individual tumor basis, the dosing schedule does influence the fluctuations in tumor size: the less frequently the drug is given, the more fluctuations there are in the tumor size (data not shown). However, this does not lead to a greater tumor size in the long-term. This result strongly suggests that it is the survival of cells at the tumor periphery, and not post-VDA angiogenesis, that is responsible for the overall failure of VDAs. If post-treatment angiogenesis was responsible for the limited efficacy of VDAs, applying the VDA over smaller time intervals would eliminate the progrowth activity encouraged by angiogenesis. Since the daily administration of the VDA did not show improved efficacy over the standard once every 3 weeks protocol, the model supports the conclusion that angiogenesis does not have a key role in VDA failure.

The unfortunate consequence of this conclusion is that the limited antitumor activity of VDAs is a result of cancer cells surviving at the tumor periphery. This is not something that can be remedied by altering the dosing schedule or the strength of the drug. Therefore, under the simplifying assumptions of

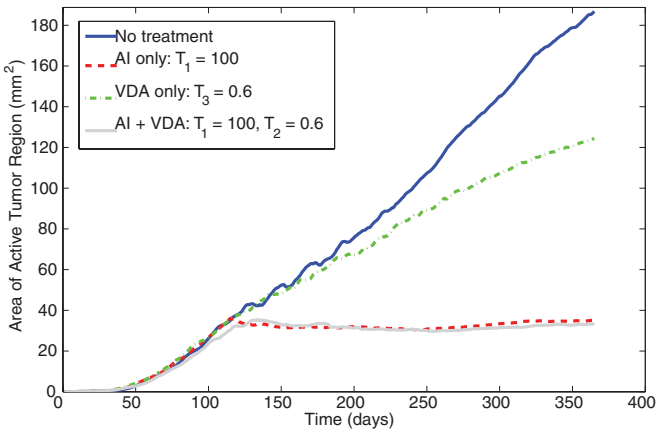

FIG. 4. (Color online) Average area of active tumor region compared for four different scenarios: no therapy is administered, AI administration only, VDA administration only, and an AI coupled with a VDA.

the model, one would conclude that for tumors growing in well-vascularized environments, VDAs will ultimately prove to be a relatively ineffective stand-alone cancer drug. It is certainly plausible that the simplifying assumptions about the vasculature are exaggerating the inefficacy of the VDA in the model. However, the model has been validated to make predictions consistent with data using preclinical and clinical dosing strategies [5]. Therefore, while the quantitative results cannot be taken too literally, the take-home message is that if a drug developer was deciding to invest in a limited set of drugs, the model suggests that AIs would be a wiser investment than VDAs (Fig. 4).

A potential caveat to this conclusion is that a VDA may enhance the efficacy of other cancer drugs. If adding a VDA to another drug protocol could enhance the action of that drug, then a VDA could still play a significant role in cancer treatment. In fact, it has been hypothesized that, given their different modes of action, targeting the tumor vasculature with AIs and VDAs is complementary rather than redundant [2]. Preclinical evidence has suggested that pairing the VDA CA4P with an anti-VEGF antibody significantly increases antitumor activity [50]. A recently completed phase I clinical trial showed that the administration of CA4P followed by bevacizumab showed "early evidence of clinical activity" [50]. Therefore, it is useful to employ the HCA model to study if there are any additive or emergent effects of administering a VDA in combination with an AI.

Figure 4 shows the average antitumor activity elicited by applying an AI every 2 weeks (always maintaining therapeutic levels) and a VDA every 3 weeks (only maintaining therapeutic levels the day the drug is given), using parameter values $T_1 = 100$ and $T_3 = 0.6$. The antitumor activity elicited by this treatment protocol is compared to previously generated data in which an AI is applied in isolation and in which a VDA is applied in isolation [5]. In Fig. 4, it can be observed that little to no benefit is gained by adding a VDA to an AI regimen.

More insight can be gained by performing a sensitivity analysis on the treatment parameters. In Fig. 5, the antitumor activity of the treatment protocol is considered at different

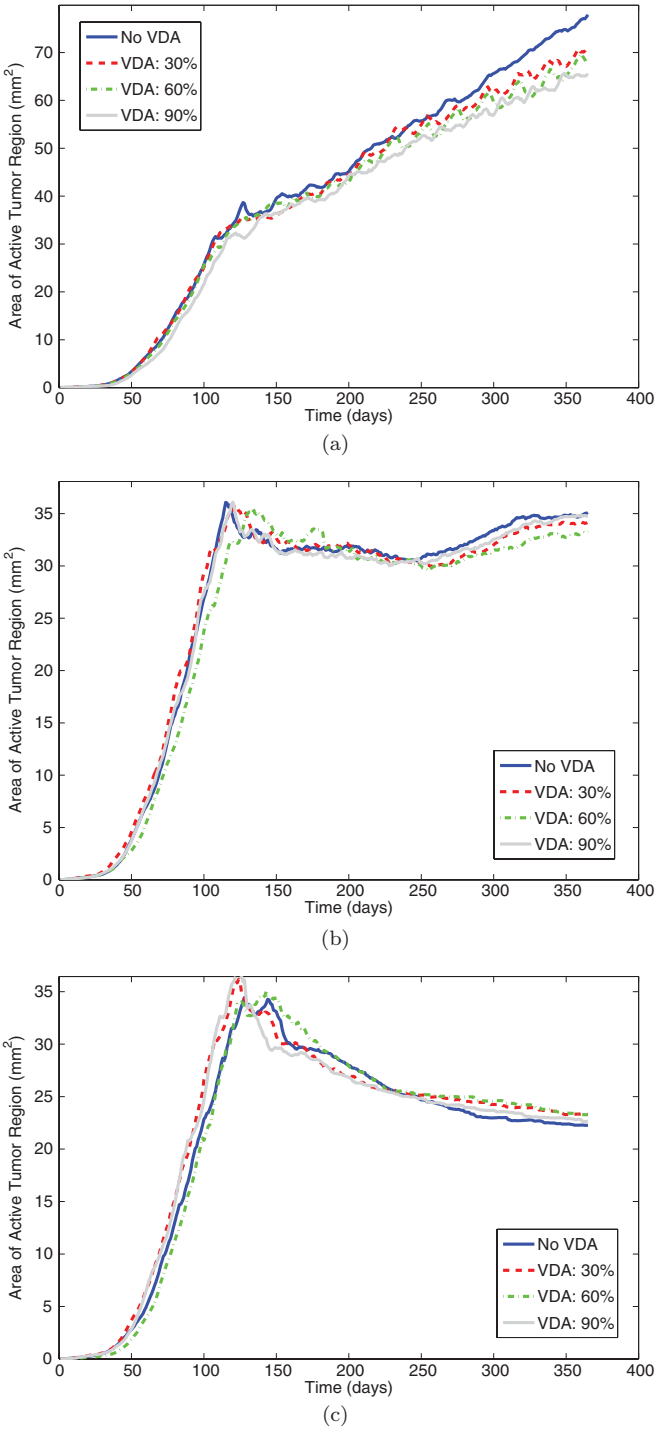

FIG. 5. (Color online) Sensitivity analysis of the AI plus VDA treatment regimen. In (a) the AI parameter is $T_1 = 10$, in (b) the AI parameter is $T_1 = 100$, and in (c) the AI parameter is $T_1 = 1000$, with the VDA taking on a range of values in each case.

AI efficacy parameters. At the lowest AI parameter tested ($T_1 = 10$), the VDA does have a noticeable impact on the average active tumor area [Fig. 5(a)]. This must be occurring because the AI has not effectively thwarted angiogenesis, leaving the VDA a substantial number of blood vessel targets. Compare this to the higher levels of AI efficacy tested ($T_1 = 100, 1000$), where the VDA exerts little to no impact

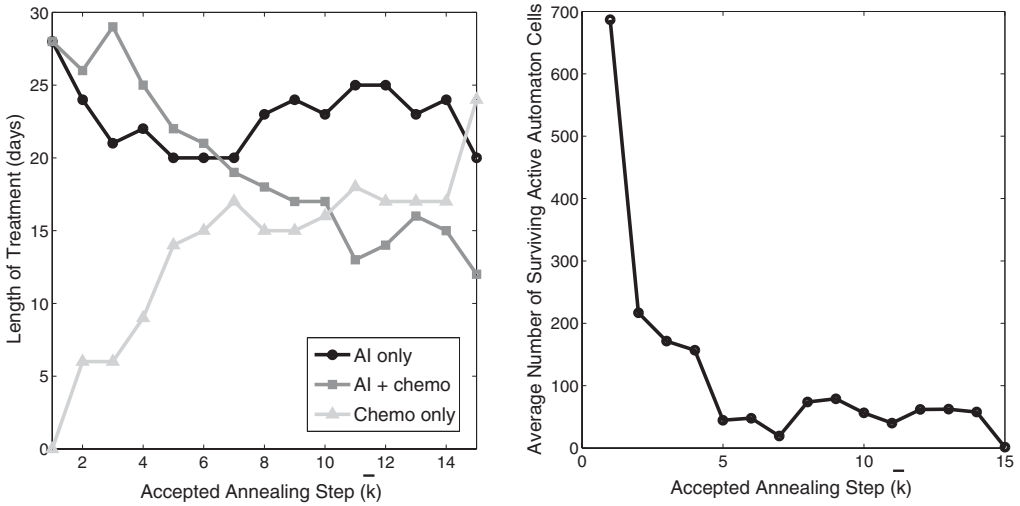

FIG. 6. Simulated annealing results. (a) Change in the treatment parameters λ_{AI}, λ_{AIC}, and λ_C as a function of accepted annealing step $\bar{k}$. $\bar{k} = N$ represents the Nth accepted parameter set. (b) Change in the average number of active cells remaining after 8 weeks of treatment as a function of accepted annealing step $\bar{k}$.

on tumor expansion because the AI very effectively inhibits angiogenesis [Figs. 5(b) and 5(c)].

Taken together, the simulations suggest that independent of the dosing schedule, VDAs have limited antitumor activity as a stand-alone drug, and minimal activity as a secondary drug added to an AI treatment regimen. As with any model predictions, this prediction is dependent on the assumptions built into the model. That said, the behavior of both AIs and VDAs in this model have been previously validated as stand-alone drugs [5]. Thus, it is certainly plausible that the biophysical model is yielding a useful conclusion for drug companies: VDAs may not be the wisest investment of a drug developer's time and money. If new data about the mode of action of VDAs (or VDAs in combination with other drugs) are uncovered, then the model assumptions will need to be revisited in this light, which may or may not alter the predictions of the algorithm.

B. Stochastic optimization of AI plus cytotoxic drug treatment protocol

A simulated annealing algorithm has been developed to identify an AI plus cytotoxic drug treatment protocol that minimizes the number of active tumor cells (proliferative plus hypoxic) after 16 weeks of treatment. In particular, the algorithm begins with an 8-week treatment protocol in which $\lambda_{AI} = 28$ (meaning therapeutic levels of AI are maintained for first 28 days) and $\lambda_{AIC} = 28$ (meaning therapeutic levels of both the AI and chemotherapeutic are maintained for the final 28 days). Initially, there is no period of time for which the cytotoxic drug is administered when the AI is not maintained at therapeutic levels ($\lambda_C = 0$). The simulated annealing scheme perturbs these three treatment times at each annealing step k as it searches for the global minimum. In Fig. 6(a), the change in the three treatment parameters is shown as a function of the *accepted* annealing step $\bar{k}$. In other words, Fig. 6(a) only shows those parameter sets that were accepted by the optimization algorithm; those parameter changes that were rejected are not shown.

One noticeable feature of the simulation results is that the treatment evolves toward a strategy in which the AI is not always maintained at therapeutic levels in the tissue. The increase in λ_C, the length of time for which the AI is not given, comes mostly at the expense of λ_{AIC}, the amount of time both the AI and chemotherapeutic are maintained at therapeutic levels [Fig. 6(a)]. The optimal treatment identified is as follows.

(1) Days 1–20: Maintain therapeutic levels of AI only ($\lambda_{AI} = 20$).

(2) Days 21–32: Maintain therapeutic levels of AI and cytotoxic chemotherapy ($\lambda_{AIC} = 12$).

(3) Days 33–56: Maintain therapeutic levels of cytotoxic chemotherapy only ($\lambda_C = 24$).

On average, this left only 1.4 active automaton cells (approximately 10 active cancer cells) remaining after 16 weeks of treatment [Fig. 6(b)]. It took 45 annealing steps, 15 of which were accepted, and 69 h of run time to identify this optimal treatment parameter set. The majority of the rejected annealing steps (and hence the run time of the algorithm) were invested in allowing the treatment strategy to accept an uphill move and evolve away from the local minimum found at $\bar{k} = 7$.

It is necessary to understand *why* this scheme has proven to be significantly more effective than the initial treatment parameter set tested. First consider the previously studied case in which an AI and chemotherapeutic are simultaneously administered, with the chemotherapeutic only administered for the maximal amount of time it can be tolerated. Using this dosing strategy, the number of proliferative cells in the simulated tumors is greatly limited [compare no treatment in Fig. 4 to the non-optimal treatment in Fig. 7(a)], in spite of the increase in tumor size upon removing the chemotherapeutic. However, a large number of quiescent hypoxic cells survive in the tumor mass. Once AI treatment ceases and oxygen conditions become more favorable, quiescent hypoxic cells can convert to a proliferative phenotype, which triggers tumor

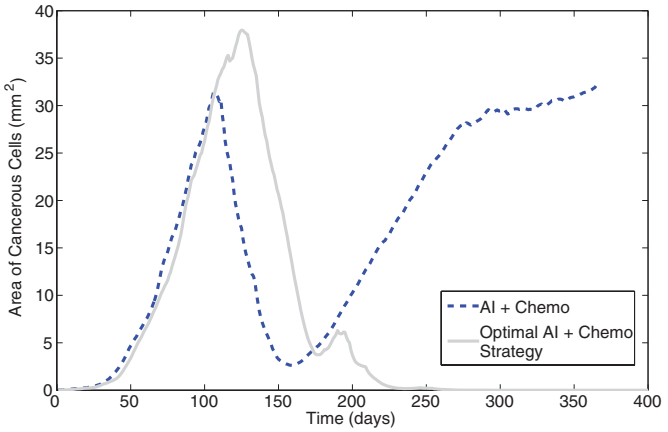

(a)

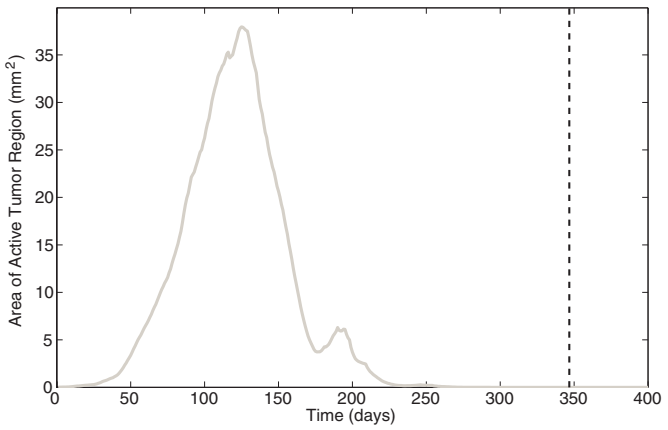

(b)

FIG. 7. (Color online) Optimal treatment strategy. (a) Comparing the efficacy of the proposed optimal treatment strategy to the simultaneous administration of an AI and a chemotherapeutic [5]. (b) Response of active tumor area to cessation of therapy. The average time of therapy cessation is denoted by a dashed black vertical line.

regrowth. This suggests that the only way to continue thwarting tumor regrowth after complete treatment cessation is to design a treatment that can destroy both proliferative and hypoxic cancer cells. This is exactly what the identified optimal treatment protocol accomplishes.

In the optimal treatment protocol identified, the AI levels in the tissue are "pulsed," meaning that therapeutic levels are maintained for a period of time, but that is followed by a period of time when therapeutic levels of the AI are no longer maintained in the tissue. By "pulsing" the AI levels in this manner, temporal bursts of angiogenesis will occur within the tumor, as there are periods in time when angiogenesis is not inhibited. These angiogenic bursts have the potential to turn hypoxic cells into proliferative ones. Since the cytotoxic agent can only target proliferative cells, this gives the cytotoxic agent a chance at a pool of cells it may not have had access to without pulsing the AI. Another way to think of this is the following: The pulsing strategy increases the access of the chemotherapeutic to the tumor mass. While the antitumor activity of an AI is a result of its ability to limit blood flow to the tumor, a secondary effect is limiting drug access to the tumor mass. Therefore, by removing the AI at predefined time intervals, and administering the chemotherapeutic during those time intervals, the chemotherapeutic has increased access to the tumor mass.

Two rounds of this optimal 8-week treatment protocol reduces the average number of proliferative and hypoxic automaton cells down to only 1.4 cells. Therefore, it is plausible that if the treatment can be applied for a few more rounds, the active tumor population can be fully eliminated by the proposed treatment protocol. In this case, cessation of treatment should not restimulate tumor growth, meaning the regrowth of simulated tumors after stopping therapy can be prevented.

To test this hypothesis, the average tumor area as a function of time is determined over the course of optimal treatment administration (Fig. 7). Importantly, while the simulated annealing scheme was run using the maximal-treatment parameter set ($T_1 = 1000, T_2 = 0.44$) in order to minimize run time, the results shown here are using a less extreme parameter set ($T_1 = 100, T_2 = 0.34$), which should be more in line with clinical parameters [5]. First and foremost, it is observed how much more successful the optimized treatment protocol is at limiting active tumor growth as compared to simply applying the AI and chemotherapeutic simultaneously for the maximum tolerated time frame [Fig. 7(a)] [5]. In and of itself, this is an important result, as this identified optimal treatment protocol has significant antitumor activity, as far as the simulated tumors are concerned.

A very important question can now be posed: What happens when all drugs stop being administered to the simulated tumors? As seen in Fig. 7(b), removing treatment after four cycles of optimal therapy does *not restimulate tumor growth*. This occurs because, on average, administering the optimal three-part treatment protocol for approximately 19 weeks was sufficient to eliminate the active tumor mass. Therefore, when the treatment is finally removed after four cycles (32 weeks), there are no more proliferative or hypoxic cells remaining in the tumor to reinitiate the growth process. Plainly stated, the simulated annealing scheme has identified a clinically attainable treatment protocol that can permanently eradicate the simulated tumors. While in no way does this suggest that a cure for cancer has been found, it does suggest that the pulsed treatment protocol may better thwart cancer progression than currently utilized dosing strategies.

C. Model shortcomings, other models, and future work

The biophysical model used herein has previously been validated in the settings of tumor growth and treatment. In terms of tumor growth, the model has been shown to quantitatively predict cancer progression when a tumor can and cannot initiate the angiogenic process [41,42]. As far as treatment is concerned, the model has been shown to qualitatively predict the antitumor activity of two vascular-targeting compounds, both with and without chemotherapy [5]. These validation studies lend credence to the predictions made by the model in novel clinical settings. However, any computational model, including the model utilized herein, has shortcomings that limit predictability. In this section, a discussion of these shortcomings is undertaken.

The underlying structure of the HCA model is the capillary network. This network is represented using a set of straight vessels with a fixed radius overlaid on a triangular lattice, subject to some optimization criterion [41]. Therefore, the network structure, while having some features of actual blood vessel networks, is not physiologically precise. Some excellent work by Welter *et al*. has been done on modeling the structure of an arterioveneous blood vessel network and how co-option of this network by a growing tumor leads to network remodeling [51,52].

Beyond the structural simplifications, the model assumes that vessel structure and blood flow are linearly related; in other words, blood flows through all vessels at the same rate, and the amount of oxygen a region of the tumor receives is directly proportional to the density of capillaries in that region. However, it is well-established that tumor vessels are dysfunctional, leaky, and highly heterogeneous [1,2], meaning that areas of high vascular density do not necessarily correspond to high oxygen levels. This property of tumor vessels has led to the paradoxical discovery that antiangiogenesis therapies can normalize the blood vessels, at least early in therapy, and therefore increase blood flow to the tumor [53]. As our model assumes that all vessels are treated equally, it cannot capture this phenomenon. A number of discrete and continuous models have incorporated the necessary details to capture this and other vessel-related phenomenon, including the effects of blood flow, wall shear stress, mechanical stress, network heterogeneities, vessel dilation and constriction, and stress-induced collapse of blood vessels [54–59]. Incorporating all of these details into the current HCA model should certainly enhance the predictive abilities of the model, although the trade-off will be a great increase in complexity. Presumably, given the previously performed validation studies on the existing model, adding these details would improve the quantitative accuracy of the model, but should not greatly alter the qualitative predictions. This is something that can certainly be explored in future work.

Another shortcoming that warrants mentioning is that both angiogenesis and cancer cell phenotype are simplified in this model. Focusing on angiogenesis first, there is only one biological pathway that leads to new vessel formation in the simulated tumors. In reality, there are many angiogenic pathways (although the VEGF pathway accounted for here is the dominant one), and treating a tumor with an AI that targets one pathway can cause a compensatory angiogenic response in the other pathways [3]. Interestingly enough, qualitative aspects of tumor response to vascular-targeting therapies can still be captured by the model without this detail. This perhaps suggests that compensatory angiogenesis is not a major factor in drug response. Another possibility is that more quantitative predictions can be made if multiple angiogenic pathways are considered in the model. Turning to cancer cell phenotype, individual tumor cells are highly evolutionary and can rapidly adapt to environmental changes, including those caused by alterations in blood flow and chemotherapy [60,61]. Previous work by Gevertz and Torquato [42] has explored the impact of the spontaneous evolution of cancer cell phenotype, and in the future, this work can be extended to study cellular adaptations induced by blood flow or chemotherapy.

The final aspect of tumor progression absent from the biophysical model is cancer cell invasion, the process whereby individual cancer cells break away from the main tumor mass and invade healthy tissue. Much insight into the invasion process has been gained using models that account for cell motility, adhesion, shape, and pressure [62–68]. The invasion process is thought to partially be driven by the oxygen and nutrient level of the tumor [69], which is a direct response to the vascular structure. Further, the invasion of cancer cells is thought to preferentially proceed along blood vessels [70]. Therefore, the process of vascular remodeling and single-cell invasion are highly dependent. As potential future work, we propose incorporating the single-cell invasion process into the HCA model of tumor growth and vessel evolution. This future work may also require altering the model to include a more physiologically accurate representation of the vessel network, possibly using a model based on the work of Rieger and colleagues [51,52]. By incorporating invasion into the biophysical model, we hope to study how the vasculature influences the invasive pattern, and how the presence of single-cell invasion influences tumor response to vascular-targeting treatments, including the optimal treatment protocol identified herein.

IV. CONCLUSIONS

In this paper, a biophysical tool has been introduced to provide a theoretical basis for helping drug design teams assess the most promising drug targets and design optimal treatment strategies. In particular, the model demonstrates that VDAs have limited antitumor activity for a wide range of dosing schedules, even when paired with an AI. While this does not rule out the possibility that VDAs can have antitumor effects through pathways not implemented in this model, it does suggest that, without further information on the action of VDAs, VDAs may not be the best investment for a drug developer trying to target tumors growing in well-vascularized environments.

The HCA model was also exploited to search for an optimal treatment protocol involving an AI, VDA, and chemotherapeutic. Given the limited efficacy of VDAs, the stochastic optimization scheme utilized focused on finding an optimal dosing strategy for the administration of an AI plus a cytotoxic chemotherapeutic. Using a simulated annealing algorithm, the model identified a "pulsed" treatment strategy that minimizes the number of active tumor cells remaining after two cycles of treatment. The identified treatment strategy is "pulsed" in that it requires that therapeutic levels of the AI are, counterintuitively, *not* maintained at all times during treatment. Follow-up simulations demonstrated that three to four rounds of optimal therapy administration yields permanent growth inhibition of the simulated tumors, even after treatment removal. While in no way does this suggest that a cure for cancer has been found, it does suggest that the pulsed treatment protocol may better thwart cancer progression than the currently utilized dosing schedule for an AI and a chemotherapeutic.

Taken together, these results demonstrate that biophysical, mathematical, and computational modeling can be used to complement the drug-development process and improve upon

current cancer treatments. For instance, our computational model strongly suggests that VDAs are not as likely to succeed in a clinical setting as AIs, at least for tumors growing in a well-vascularized environment. Armed with this sort of knowledge, drug developers could divert their resources away from VDAs and instead focus on more promising cancer therapies like AIs. Further, the model can be used to design dosing protocols for clinical trial studies. As an example, the pulsed AI and chemotherapy strategy discovered herein could be one of the dosing schedules tested in a clinical trial. For these reasons and others, mathematical and biophysical modeling holds the promise of changing what drugs are developed, how these drugs are tested, and how we treat cancer patients.

APPENDIX: BIOPHYSICAL MODEL—THE DETAILS

The algorithm utilized in this paper is a slightly modified version of the algorithm proposed by Gevertz and Torquato [41]. Besides these small modifications, which are detailed below, the algorithm has also been adopted to account for the administration of a drug at predefined time intervals. The skeleton framework of the algorithm is summarized in Algorithm 1.

Algorithm I. HCA model of vascular tumor growth and treatment

INPUT: Cell and vessel location in tissue region
while time $< T_{\max}$ do
STEP 1: Numerically solve system of PDEs
STEP 2: Determine vessel response to PDE solution
STEP 3: Evolve each automaton cell
STEP 4: Apply treatment (if treatment is given at this time)
end while

(i) *Automaton cell generation*. A Voronoi tessellation of random points generated using the nonequilibrium procedure of random sequential addition of hard disks determines the underlying lattice for the algorithm [41,71]. Each automaton cell created via this procedure represents a cluster of biological cells. Assuming the tumor under consideration is GBM (in which glial cells have an average diameter of 40 μm [72]), each automaton cell is chosen to represent a cluster of seven glial cells. This number is small enough to give an average automaton cell diameter less than the characteristic diffusion length of oxygen, but large enough to keep the run time of the algorithm manageable [41].

(ii) *Healthy microvascular network*. The blood vessel network which supplies the cells in the tissue region of interest with oxygen and nutrients must be generated. This is done using a modification of the Krogh cylinder model; a model of the capillary network which assumes that capillaries are straight, parallel, and uniformly spaced [73]. The random analog proposed by Gevertz and Torquato takes the idea of using parallel line segments and randomizes it, subject to a set of biologically inspired constraints. In particular, linear blood vessels are sequentially attempted to be placed within the tissue region of interest. A vessel can only be added to the system, however, if it is not too close to a parallel vessel, if it does not cause too many vessels to intersect at one site, and if it vascularizes at least one unvascularized cell [41].

(iii) *Initialize tumor*. Designate the automaton cell in the center of the tissue space as a proliferative cancer cell. This is equivalent to taking the nonmalignant cell in the center of the tissue and endowing it with a malignant phenotype.

(iv) *Tumor growth algorithm*. Time is then discretized into units that represent 1 real day. At each time step:

(a) *Solve PDEs*. The following previously developed system of PDEs [41] is numerically solved 1 day forward in time:

$$\frac{\partial v}{\partial t} = D_v \Delta v + b_v h_i (h - v^2/K_v) - k_0 v r_{v0} + k_{-0} r_v - \mu_v v, \tag{A1}$$

$$\frac{\partial a_1}{\partial t} = b_{a1} e_i (p_i + h_i + n_i)\left(e_0 - a_1^2/K_a\right) - k_1 a_1 r_{a0} + k_{-1} r_{a1} - \mu_{a1} a_1, \tag{A2}$$

$$\frac{\partial a_2}{\partial t} = D_{a2} \Delta a_2 + b_{a2} e_i (p_i + h_i + n_i)\left(e_0 - a_2^2/K_a\right) + \bar{b}_{a2} h_i \left(h - a_2^2/K_a\right) - k_2 a_2 r_{a0} + k_{-2} r_{a2} - \mu_{a2} a_2, \tag{A3}$$

$$\frac{\partial r_{v0}}{\partial t} = -k_0 v r_{v0} + k_{-0} r_v, \tag{A4}$$

$$\frac{\partial r_{a0}}{\partial t} = -k_1 a_1 r_{a0} + k_{-1} r_{a1} - k_2 a_2 r_{a0} + k_{-2} r_{a2}, \tag{A5}$$

$$\frac{\partial r_v}{\partial t} = k_0 v r_{v0} - k_{-0} r_v, \tag{A6}$$

$$\frac{\partial r_{a1}}{\partial t} = k_1 a_1 r_{a0} - k_{-1} r_{a1}, \tag{A7}$$

$$\frac{\partial r_{a2}}{\partial t} = k_2 a_2 r_{a0} - k_{-2} r_{a2}. \tag{A8}$$

In these equations, v represents the concentration of VEGF, r_{v0} is the concentration of the unbound VEGFR-2, and r_v is the VEGFR-2 receptor bound by VEGF. Further, the concentration of Ang-1 is given by a_1, that of Ang-2 is given by a_2, that of unoccupied Tie-2 is given by r_{a0}, that of Tie-2 bound by Ang-1 is given by r_{a1}, and that of Tie-2 bound by Ang-2 is given by r_{a2}.

For the three ligands (VEGF, Ang-1, and Ang-2) each equation indicates that the protein is produced by the appropriate cell type (with a carrying capacity term [46]) and that there is a linear decay term. Both VEGF and Ang-2 diffuse, whereas Ang-1 does not. This is because Ang-1 is produced by ECs and then acts in a paracrine manner upon these ECs [46]. Further, the source term of each protein depends on the cell types that produce the protein. VEGF is produced by hypoxic cells [46] (h_i, where h stands for hypoxia and the subscript i denotes

that this is an indicator function), Ang-2 is produced by ECs associated with malignant tissue (this includes ECs associated with proliferative cells p, necrotic cells n, and hypoxic cells) and is also produced by hypoxic cells [46], and Ang-1 is produced by ECs associated with malignant tissue.

For each receptor (VEGFR-2 and Tie-2), the equation represents the association and dissociation of the ligand-receptor complex. The schematic in Fig. 2 graphically illustrates the processes being modeled in Eqs. (A1)–(A8). A complete list of variable and parameter definitions, along with details on the stable finite difference scheme used to solve the differential equations can be found elsewhere [5,41].

(b) *Vessel evolution*. Check whether each vessel meets the requirements for regression or growth. Vessels with a concentration of bound Ang-2 six times greater than that of bound Ang-1 regress [44], provided that the concentration of bound VEGF is below its critical value. Vessel tips with a sufficient amount of bound VEGF sprout along the VEGF gradient.

(c) *Nonmalignant cells*. Healthy cells undergo apoptosis if vessel regression causes its oxygen concentration to drop below a critical threshold. To simulate this, a characteristic diffusion length of nutrients in tissue of 250 μm is used [26,74], and it is assumed that oxygen can only reach cells within this critical distance from a blood vessel. Therefore, it is supposed that if the distance of a healthy cell from a blood vessel exceeds $l_{\text{prolif}} = 250$ μm, then the oxygen level at that cell is insufficient, and the cell undergoes apoptosis. Further, nonmalignant cells do not divide in the model, which is a reasonable assumption for GBM [75].

(d) *Inert cells*. Tumorous necrotic cells are inert.

(e) *Hypoxic cells*. A hypoxic cell turns proliferative if it is within a distance of $l_{\text{prolif}} = 250$ μm from a blood vessel. This is equivalent to saying its oxygen level exceeds a specified threshold [41]. Similarly, a hypoxic cell turns necrotic if the oxygen level drops below a specified threshold. This is implemented by converting any hypoxic cell that is further than a distance of $l_{\text{hyp}} = 1500$ μm from a vessel into a necrotic cell [41].

(f) *Proliferative cells*.

(1) A proliferative cell turns hypoxic if its oxygen level drops below a specified threshold; that is, if it is further than a distance of $l_{\text{prolif}} = 250$ μm from a blood vessel.

(2) If the oxygen level at a proliferative cell is sufficiently high, the cell *may* attempt to divide into the space of a viable nonmalignant cell. To determine the position of the daughter cell, an intercellular mechanical stress growth process is assumed [71]. In this process, the new proliferative cell is placed in the position of the dividing cells nearest neighbor. If this cell is occupied (meaning, if a cancer cell is already located at this nearest neighbor site), the tumor cells are successively pushed outward, eventually resulting in the presence of one new proliferative automaton cell at the tumor periphery.

(3) The probability that a proliferative cell divides, p_{div}, is influenced by the location of the dividing cell from the tumor center (r), reflecting the effects of mechanical confinement pressure imposed by the skull. In particular, assuming a maximum tumor extent of R_{max} (taken to be 10 mm in the model), and assuming that mechanical confinement pressure inhibits tumor growth, gives the following equation for p_{div}:

$$p_{\text{div}} = p_0 \left(1 - \frac{r}{R_{\text{max}}}\right). \tag{A9}$$

The base probability of division, p_0, depends on the distance of the cell to the nearest blood vessel, d_{vessel}. The average value of p_0 was fixed to be 0.192 (corresponding to a cell doubling time of approximately four days), with p_0 taking on a minimum value $p_{\text{min}} = 0.1$ and a maximum value $p_{\text{max}} = 0.284$ [42]. This means that a proliferative cell in the model can have a cell doubling time anywhere in the range of 3 to 7 days. The formula used to determine p_0 is

$$p_0 = \frac{p_{\text{min}} - p_{\text{max}}}{l_{\text{prolif}}} d_{\text{vessel}} + p_{\text{max}}, \tag{A10}$$

where $d_{\text{vessel}} \leqslant 250$ since only well-oxygenated cells can divide. Under this condition, $p_0 > 0$.

(v) *Apply treatment* (if applicable on a particular day).

[1] P. E. Thorpe, Clin. Cancer Res.**10**, 415 (2004).

[2] D. W. Siemann, in *Vascular-targeted Therapies in Oncology* (Wiley & Sons, West Sussex, England, 2006), pp. 1–8.

[3] G. Bergers and D. Hanahan, Nat. Rev. Cancer **8**, 592 (2008).

[4] M. M. Cooney, J. Ortiz, R. M. Bukowski, and S. C. Remick, Curr. Oncol. Rep. **7**, 90 (2005).

[5] J. L. Gevertz, Comput. Math. Methods Med. **2011**, 830515 (2011).

[6] M. Dickson and J. P. Gagnon, Nat. Rev. Drug Discovery **3**, 417 (2004).

[7] C. P. Adams and V. V. Brantner, Health Aff. **25**, 420 (2006).

[8] J. Gabrielsson and D. Weiner, *Pharmacokinetic and Pharmacodynamic Data Analysis: Concepts and Applications* 3rd ed. (Swedish Pharmaceutical Press, Stockholm, 2000).

[9] A. Iliadis and D. Barbolosi, Comput. Biomed. Res. **33**, 211 (2000).

[10] K. R. Fister and J. C. Panetta, SIAM J. Appl. Math. **60**, 1059 (2000).

[11] D. Barbolosi and A. Iliadis, Comput. Biol. Med. **31**, 157 (2001).

[12] K. R. Fister and J. C. Panetta, SIAM J. Appl. Math. **63**, 1954 (2003).

[13] J. J. Grudzinski, W. Tomé, J. P. Weichert, and R. Jeraj, Phys. Med. Biol. **55**, 5723 (2010).

[14] B. Ribba, K. Marron, Z. Agur, T. Alarcón, and P. K. Maini, Bull. Math. Biol. **67**, 79 (2005).

[15] J. P. Sinek, S. Sanga, X. Zheng, H. B. Frieboes, M. Ferrari, and V. Cristini, J. Math. Biol. **58**, 485 (2009).

[16] T. L. Jackson, J. Math. Biol. **44**, 201 (2002).

[17] A. Bertuzzi, A. D'Onofrio, A. Fasano, and A. Gandolfi, Bull. Math. Biol. **65**, 903 (2003).

[18] S. C. Ferreira, M. L. Martins, and M. J. Vilela, Phys. Rev. E **67**, 051914 (2003).

[19] E. S. Norris, J. R. King, and H. M. Byrne, Math. Comput. Model. **43**, 820 (2006).

[20] P. Tracqui, Rep. Prog. Phys. **72**, 056701 (2009).

[21] L. G. De Pillis and A. Radunskaya, J. Theor. Med. **3**, 79 (2001).

[22] S. A. Menchón and C. A. Condat, Eur. Phys. J. Spec. Top. **143**, 89 (2007).

[23] K. R. Swanson, J. E. C. Alvord, and J. D. Murray, Acta. Biotheor. **50**, 223 (2002).

[24] H. B. Frieboes, M. E. Edgerton, J. P. Fruehauf, F. R. A. J. Rose, L. K. Worrall, R. A. Gatenby, M. Ferrari, and V. Cristini, Cancer Res. **69**, 4484 (2009).

[25] D. Y. Arifin, K. Y. T. Lee, and C.-H. Wang, J. Controlled Release **33**, 211 (2009).

[26] J. Sinek, H. Frieboes, X. Zheng, and V. Cristini, Biomed. Microdevices **6**, 297 (2004).

[27] M. Abundo and C. Rossi, J. Math. Biol. **27**, 81 (1989).

[28] M. I. S. Costa, J. L. Boldrini, and R. C. Bassanezi, Math. Biosci. **125**, 211 (1995).

[29] J. R. Usher and D. Henderson, Math. Med. Biol. **13**, 99 (1996).

[30] J. L. Boldrini and M. I. S. Costa, Math. Med. Biol. **17**, 33 (2000).

[31] B. Titz and R. Jerag, Phys. Med. Biol. **53**, 4471 (2008).

[32] C. Harting, P. Peschke, K. Borkenstein, and C. P. Karger, Phys. Med. Biol. **52**, 4775 (2007).

[33] G. Powathil, M. Kohandel, S. Sivaloganathan, A. Oza, and M. Milosevic, Phys. Med. Biol. **52**, 3291 (2007).

[34] L. Arakelyan, V. Vainstein, and Z. Agur, Angiogenesis **5**, 203 (2002).

[35] A. Ergun, K. Camphausen, and L. M. Wein, Bull. Math. Biol. **65**, 407 (2003).

[36] A. d'Onofrio and A. Gandolfi, Math. Biosci. **191**, 159 (2004).

[37] U. Ledzewicz and H. Schättler, SIAM J. Control Optim. **46**, 1052 (2007).

[38] M. Kohandel, M. Kardar, M. Milosevic, and S. Sivaloganathan, Phys. Med. Biol. **52**, 3665 (2007).

[39] J. Panovska, H. M. Byrne, and P. K. Maini, Math. Comput. Model. **47**, 560 (2008).

[40] P. Hinow, P. Gerlee, L. J. McCawley, V. Quaranta, M. Ciobanu, S. Wang, J. M. Graham, B. P. Ayati, J. Claridge, K. R. Swanson *et al.* , Math. Biosci. Eng. **6**, 521 (2009).

[41] J. L. Gevertz and S. Torquato, J. Theor. Biol. **243**, 517 (2006).

[42] J. L. Gevertz and S. Torquato, Phys. Rev. E **80**, 051910 (2009).

[43] J. Holash, P. C. Maisonpierre, D. Compton, P. Boland, C. R. Alexander, D. Zagzag, G. D. Yancopoulos, and S. J. Weigand, Science **284**, 1994 (1997).

[44] C. S. Maisonpierre, C. Suri, P. F. Jones, S. Bartunkova, S. J. Wiegand, C. Radziejewski, D. Compton, J. McClain, T. H. Aldrich, N. Papadlopoulous *et al.* , Science **277**, 55 (1997).

[45] R. A. Brekken and P. E. Thorpe, J. Controlled Release **74**, 173 (2001).

[46] V. Tse, L. Xu, Y. C. Yung, J. G. Santarelli, D. Juan, K. Fabel, G. Silverberg, and G. Harsh IV, Neurol. Res. **25**, 729 (2003).

[47] J.-F. Lu, R. Bruno, S. Eppler, W. Novotny, and J. Gaudreault, Cancer Chemother. Pharmacol. **62**, 779 (2008).

[48] R. Stupp, P. Y. Dietrich, S. Ostermann Kraljevic, A. Pica, I. Maillard, P. Maeder, R. Meuli, R. Janzer, G. Pizzolato, R. Miralbell *et al.*, J. Clin. Oncol. **20**, 1375 (2002).

[49] S. Torquato, *Random Heterogeneous Materials: Microstructure and Microscopic Properties* (Springer-Verlag, New York, 2002).

[50] P. D. Nathan, I. Judson, A. Padhani, A. Harris, C. P. Carden, J. Smythe, D. Collins, M. Leach, P. Walicke, and G. J. Rustin, J. Clin. Oncol. **26(Suppl.)**, 3550 (2008).

[51] M. Welter, K. Bartha, and H. Rieger, J. Theor. Biol. **259**, 405 (2009).

[52] M. Welter and H. Rieger, Eur. Phys. J. E **33**, 149 (2010).

[53] R. K. Jain, Nat. Med. **7**, 987 (2001).

[54] T. Alarcón, H. M. Byrne, and P. K. Maini, Prog. Biophys. Mol. Biol. **85**, 451 (2004).

[55] T. Alarcón, H. M. Byrne, and P. K. Maini, Multiscale Model. Simul. **3**, 440 (2005).

[56] S. R. McDougall, A. R. A. Anderson, and M. A. J. Chaplain, J. Theor. Biol. **241**, 564 (2006).

[57] A. L. Bauer, T. L. Jackson, and Y. Jiang, Biophys. J. **92**, 3105 (2007).

[58] M. Welter, K. Bartha, and H. Rieger, J. Math. Biol. **250**, 257 (2008).

[59] P. Macklin, S. McDougall, A. R. Anderson, M. A. Chaplain, and J. Lowengrub, J. Math. Biol. **58**, 765 (2009).

[60] N. Raghunand, R. A. Gatenby, and R. J. Gillies, Br. J. Radiol. **76**, S11 (2003).

[61] J. C. Cusack, Cancer Treat. Rev. **29**, 21 (2003).

[62] S. Turner and J. A. Sherratt, J. Theor. Biol. **216**, 85 (2002).

[63] H. B. Frieboes, X. Zheng, C.-H. Sun, B. Tromberg, R. Gatenby, and V. Cristini, Cancer Res. **66**, 1597 (2006).

[64] A. M. Stein, T. Demuth, D. Mobley, M. Berens, and L. M. Sander, Biophys. J. **92**, 356 (2007).

[65] B. M. Rubenstein and L. J. Kaufman, Biophys. J. **95**, 5661 (2008).

[66] K. J. Painter, J. Math. Biol. **58**, 511 (2009).

[67] A. R. Anderson, K. A. Rejniak, P. Gerlee, and V. Quaranta, J. Math. Biol. **58**, 579 (2009).

[68] Y. Jiao and S. Torquato, PLoS Comput. Biol. **7**, e1002314 (2011).

[69] S. L. C. Lee, P. Rouhia, L. D. Jensena, D. Zhanga, H. Jia, G. Hauptmannc, P. Inghamb, and Y. Caoa, Proc. Natl. Acad. Sci. USA **106**, 19485 (2009).

[70] P. Gritsenko, O. Ilina, and P. Friedl, J. Pathol. **226** 185 (2012).

[71] A. R. Kansal, S. Torquato, R. G. Harsh IV, E. A. Chiocca, and T. S. Deisboeck, J. Theor. Biol. **203**, 367 (2000).

[72] W. C. Broaddus, P. J. Haar, and G. T. Gillies, in *Encyclopedia of Biomaterials and Biomedical Engineering*, 3rd ed. (Dekker, New York, 2004), pp. 1035–1042.

[73] J. E. Fletcher, Math. Biosci. **38**, 159 (1978).

[74] X. Zheng, S. M. Wise, and V. Cristini, Bull. Math. Biol. **67**, 211 (2005).

[75] J. L. Gevertz, G. T. Gillies, and S. Torquato, Phys. Biol. **5**, 036010 (2008).